Bioorganic & Medicinal Chemistry 23 (2015) 7069–7078

Contents lists available at ScienceDirect

Bioorganic & Medicinal Chemistry

journal homepage: www.elsevier.com/locate/bmc

5-Lipoxygenase inhibitors suppress RANKL-induced osteoclast formation via NFATc1 expression

Ju-Hee Kang [a], Zheng Ting [a], Mi-ran Moon [a], Jung-Seon Sim [a], Jung-Min Lee [a], Kyung-Eun Doh [c], Sunhye Hong [c], Minghua Cui [c], Sun Choi [c], Hyeun Wook Chang [b], Hea-Young Park Choo [c,*], Mijung Yim [a,*]

[a] College of Pharmacy, Sookmyung Women's University, Seoul 140-742, Republic of Korea
[b] College of Pharmacy, Yeungnam University, Gyeongsan 712-749, Republic of Korea
[c] College of Pharmacy, Graduate School of Pharmaceutical Sciences, and Global Top 5 Research Program, Ewha Womans University, Seoul 120-750, Republic of Korea

ARTICLE INFO

Article history:
Received 5 July 2015
Revised 14 September 2015
Accepted 15 September 2015
Available online 15 September 2015

Keywords:
5-Lipoxygenase
Benzoxazole scaffold
RANKL-induced osteoclast formation
NFATc1
Lipopolysaccharide (LPS)-induced osteoclast formation

ABSTRACT

5-Lipoxygenase synthesizes leukotrienes from arachidonic acid. We developed three novel 5-LO inhibitors having a benzoxazole scaffold as a potential anti-osteoclastogenics. They significantly suppressed RANKL-induced osteoclast formation in mouse bone marrow-derived macrophages. Furthermore, one compound, **K7**, inhibited the bone resorptive activity of osteoclasts. The anti-osteoclastogenic effect of **K7** was mainly attributable to reduction in the expression of NFATc1, an essential transcription factor for osteoclast differentiation. **K7** inhibited osteoclast formation via ERK and p38 MAPK, as well as NF-κB signaling pathways. **K7** reduced lipopolysaccharide (LPS)-induced osteoclast formation in vivo, corroborating the in vitro data. Thus, **K7** exerted an inhibitory effect on osteoclast formation in vitro and in vivo, properties that make it a potential candidate for the treatment of bone diseases associated with excessive bone resorption.

1. Introduction

Osteoclasts are multinucleated cells derived from the monocyte-macrophage lineage of hematopoietic precursors.[1] Osteoclasts are bone-resorbing cells and increased numbers of osteoclasts can lead to the development of diseases characterized by bone loss, such as osteoporosis, rheumatoid arthritis, Paget's disease, periodontal disease, osteosarcoma, and cancer bone metastasis.[2–5] Pharmaceutical inhibition of osteoclast differentiation is considered a promising therapeutic strategy for the prevention of bone loss-associated disorders and related fractures.

Osteoclast differentiation is primarily regulated by two cytokines: macrophage-colony stimulating factor (M-CSF) and receptor activator of nuclear factor-κB ligand (RANKL). The binding of M-CSF to its receptor, M-CSFR on the surface of osteoclast precursor induces surface expression of RANK (a receptor of RANKL). The binding of RANKL to RANK triggers activation of signaling molecules, including mitogen-activated protein kinases (MAPKs) and NF-κB that then evoke downstream activation of c-Fos and nuclear factor of activated T cells c1 (NFATc1).[6] c-Fos is an essential factor for induction of NFATc1, a master transcription factor of osteoclast-specific genes and therefore of osteoclast differentiation.[7]

5-Lipoxygenase (5-LO) is a crucial enzyme of the arachidonic acid (AA) cascade catalyzing the formation of bioactive leukotrienes (LTs). 5-LO catalyzes the conversion of AA to 5(*S*)-hydroperoxyeicosatetraenoic acid (5-HPETE) and leukotriene (LT)A_4.[8,9] The intermediate LTA_4 can be further converted to LTB_4 by LTA_4 hydrolase[10] or to LTC_4 by LTC_4 synthase.[11] 5-LO-derived AA metabolites represent potent mediators of inflammatory reactions. In recent years, accumulating evidence indicates that the 5-LO pathway plays a role in the development of allergic diseases, such as asthma,[12] and a variety of inflammatory disorders, such as rheumatoid arthritis.[13] Furthermore, the 5-LO pathway also plays a key role in bone metabolism. Genetic loss of 5-LO activity alters bone morphology,[14] and increases cortical bone thickness.[15]

Abbreviations: 5-LO, 5-lipoxygenase; LTs, leukotrienes; BMMs, bone marrow-derived macrophages; BMMCs, bone marrow-derived mast cells; LPS, lipopolysaccharide; M-CSF, macrophage-colony stimulating factor; RANK, a receptor of RANKL; RANKL, receptor activator of nuclear factor-κB ligand; ERK, extracellular signal-regulated kinases; MAPKs, mitogen-activated protein kinases; NFATc1, nuclear factor of activated T cells c1; TRAP, tartrate-resistant acid phosphatase; $TRAP^+$, tartrate-resistant acid phosphatase positive; MNCs, multinucleated cells; DC-STAMP, dendritic cell-specific transmembrane protein; Atp6vod2, D2 isoform of vacuolar (H+) ATPase (v-ATPase) V_o domain; CTR, calcitonin receptor.

* Corresponding authors.
E-mail addresses: hypark@ewha.ac.kr (H.-Y. Park Choo), myim@soomyung.ac.kr (M. Yim).

http://dx.doi.org/10.1016/j.bmc.2015.09.025
0968-0896/

Leukotrienes produced via 5-LO can stimulate osteoclast formation and activity, suggesting that the increased cortical thickness found in 5-LO knockout mice may be associated with reduced osteoclast number and activity.[16–18] Thus 5-LO inhibitors are of therapeutic value for the treatment or prevention of bone related-diseases.

The 5-LO protein consists of a C-terminal catalytic domain and an N-terminal C2-like β-barrel domain.[19] The catalytic domain contains a non-heme iron in the active site that acts as an electron acceptor or donor during catalysis.[20] During enzyme activation, the iron is oxidized from the ferrous state (Fe^{2+}) to the ferric (Fe^{3+}) form, thus gaining entry in the catalytic cycle. The C2-like domain has a regulatory function. Most 5-LO inhibitors bind to the catalytic site of the enzyme and exhibit varying efficiencies of competitive inhibition.[21] Zileuton, *N*-[1-(1-benzothien-2-yl)ethyl]-*N*-hydroxyurea, is the first and only approved 5-LO inhibitor to date. However, it only partially inhibits the synthesis of leukotrienes at clinical dose and the therapeutic index is limited by side-effects.[22] Currently, there is no drug available that completely inhibits the actions of all the 5-LO-induced mediators. Therefore, there is a need for the development of new inhibitors with a pharmacological profile of high potency of enzyme inhibition.

Recently we reported the design and synthesis of a series of benzoxazoles and benzothiazoles as 5-LO inhibitors.[23,24] In our continuing effort, we synthesized the novel three compounds having a benzoxazole scaffold, investigated as a potential anti-osteoclastogenics using mouse bone marrow-derived macrophages (BMMs) in this study. Furthermore, we selected one compound **K7**, evaluated the pharmacological effect of **K7** on osteoclast formation, in vitro and in vivo. Our findings suggested that **K7** could be used as a new therapeutic agent against bone lytic diseases involving increased osteoclastogenesis.

2. Results

2.1. Synthesis of (5-(4-(*N*′-hydroxycarbaimidoyl)-phenoxy)-*N*-(2-(4-substituted phenylamino)benzo[*d*]oxazole-5-yl)pentanamide (5a–c) and their 5-LO inhibition

Chemical synthesis of benzoxazole derivatives is delineated in Scheme 1. The synthesis of starting compounds was reported in previous study.[24] Briefly, 5-nitro-2-aminophenol was reacted with ethylphenyl isothiocyanate to give the corresponding thiourea, then benzoxazoles (**1a–c**) were prepared by KO_2 catalyzed ring closure. The nitro compounds **1a–c** were reduced to amino compounds **2a–c** by 5% Pd/C and hydrogen. Coupling of amino group and 5-bromovaleric acid by PyBOP resulted in the amides **3a–c**. Reaction of **3a–c** and 4-cyanophenol under K_2CO_3 produced **4a–c**, and the following reaction with NH_2OH gave rise to the final compounds **5a–c** (Scheme 1).

5-LO inhibition was measured as the formation of LTC_4 in the bone marrow-derived mast cells as explained in a previous study.[24] The ability of compounds **5a**, **5b** and **5c** to inhibit 5-LO (IC_{50}) were 1.72, 4.10, and 4.90 μM respectively.

2.2. Molecular modeling

To investigate the binding interactions of most active compound **5a** (**K7**) in 5-LO, we performed the docking study using the human X-ray crystal structure (PDB ID: 3V99).[25] As shown in Figure 1, the 4-ethylaniline group nicely fitted into the bottom hole at the active site, forming the hydrophobic interactions with Phe555, Phe610, and Tyr660. The benzene ring of the benzoxazole group participated in hydrophobic interactions with Phe555, Leu607, and Phe610. The amide NH was able to form hydrogen bonding with Ala672. The phenoxy phenyl ring made the π–π stacking with Phe177 and also involved in the hydrophobic interactions with Phe177 and Ala410 in the upper region of the binding site. Furthermore, the nitrogen of carbamimidoyl amine formed hydrogen bonding with Ala410.

2.3. Inhibition of RANKL-induced osteoclast formation and bone resorption in vitro

To check the effect of **5a–c** on RANKL-induced osteoclast formation, we used a mouse bone marrow-derived macrophages (BMMs) culture system. BMMs can differentiate into tartrate-resistant acid phosphatase positive ($TRAP^+$) multinucleated osteoclasts in the presence of M-CSF and RANKL. BMMs were cultured with various concentrations of three compounds. $TRAP^+$ multinucleated cells (MNCs) containing more than 3 or 5 nuclei, >100 μm in diameter, were counted as mature osteoclasts. IC_{50} of **5a**, **5b** and **5c** were 1.31, 0.56, and 0.58 μM, respectively, which is more effective than zileuton (>20 μM). **5a** (**K7**) suppressed the RANKL-induced osteoclast formation in a dose-dependent manner, with complete inhibition at 10 μM (Fig. 2A). **K7** did not affect cell proliferation, suggesting that the anti-osteoclastogenic effect of **K7** was not attributable to cellular proliferation (Fig. 2B). Bone resorption is a unique function of osteoclasts, generating resorption pits on bone.[26] To examine whether the effect of **K7** on osteoclast formation extended to osteoclastic function, we performed an in vitro resorption pit assay using the dentin slice. Many resorption pits were generated in wells with RANKL-treated osteoclasts. In

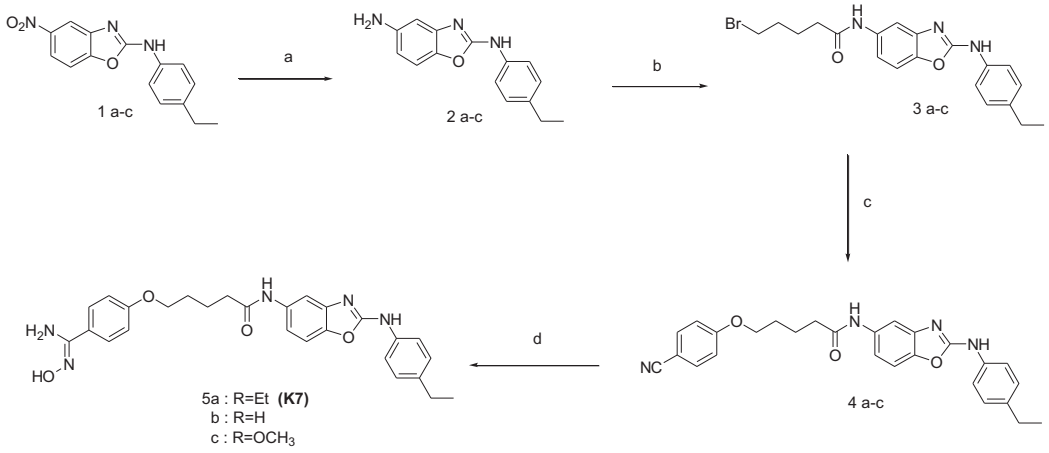

Scheme 1. Reagents and conditions: (a) 5% Pd/C, H_2, CH_3OH, room temperature, 24 h, (b) 5-bromovaleric acid, PyBOP, $^iPr_2NEt$, DMF, room temperature, 16 h, (c) 4-cyanophenol, K_2CO_3, DMF, 60 °C, 5 h, (d) CH_3OH, NH_2OH 50% in water, 40 °C, 16 h.

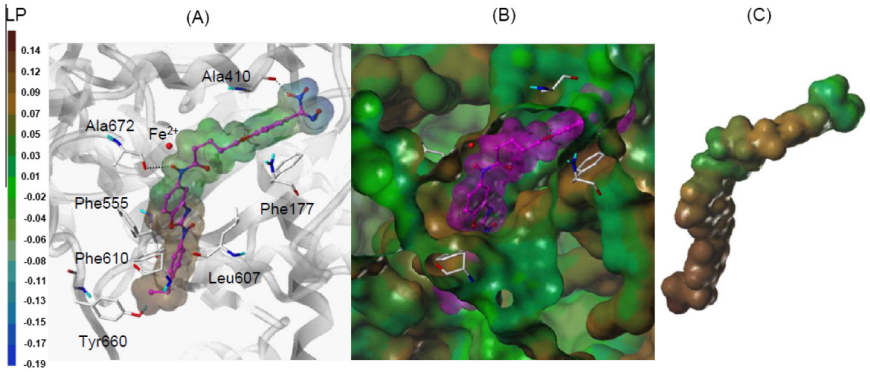

Figure 1. Docking result of **K7** in the human 5-lipoxygenase. (A) Predicted binding interactions of **K7** at the active site of h5-LO. The key interacting residues are labeled and shown as capped-stick with their carbon atoms in white color. The ferrous ion (Fe^{2+}) is displayed as a ball in red-orange color. The secondary structure of h5-LO is colored with gray. **K7** is displayed in ball-and-stick with the carbon atoms in magenta color. The van der Waals surface of **K7** is colored by the lipophilic potential. Hydrogen bonds are shown in black dashed lines. (B) The Fast Connolly surface of h5-LO and the van der Waals surface of **K7**. Molecular surface of h5-LO was created by MOLCAD and presented with the lipophilic potential. The surface of h5-LO is Z-clipped for clarity, and that of **K7** is in magenta color. (C) Van der Waals surface of the docked **K7** is colored by the lipophilic potential.

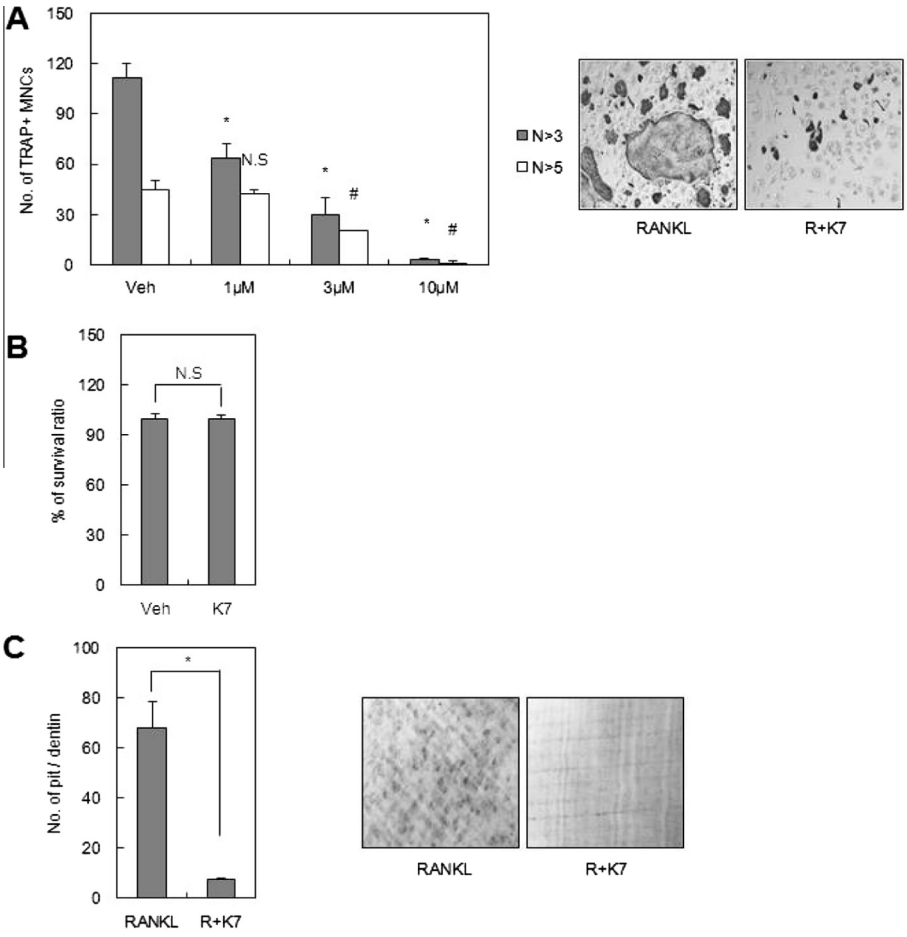

Figure 2. **K7** inhibits RANKL-induced osteoclast formation and bone resorption. (A) BMMs were cultured with RANKL (100 ng/mL) and M-CSF (30 ng/mL) in the absence or presence of **K7** at the indicated concentrations for 4 days. Cells were fixed and stained for TRAP and $TRAP^{+}$ MNCs containing more than 3 or 5 nuclei were counted. (B) BMMs were cultured with or without **K7** (10 μM) and M-CSF for 4 days, and the cell number was assessed by MTT assay. (C) BMMs were differentiated on dentine slices with M-CSF (30 ng/mL) and RANKL (100 ng/mL) for 4 days, and then **K7** (10 μM) was treated for 2 days in the presence of M-CSF and RANKL. The remaining cells were removed and stained with toluidine blue. The resorbed pit numbers were counted. Veh, vehicle; R, RANKL; N.S., not significant (*, $^{\#}p$ <0.05 vs Veh). Data are expressed as mean ± SD of three independent experiments.

contrast, the treatment of **K7** strongly inhibited formation of resorption pits by the RANKL-treated osteoclasts (Fig. 2C). Together, these results suggested that **K7** exerted inhibitory effects on osteoclast formation and function, which eventually translated to reduced bone resorption.

2.4. Osteoclastogenic genes expression

RANKL induces many target genes responsible for osteoclast differentiation and function.[27] For example, osteoclasts fuse via dendritic cell-specific transmembrane protein (DC-STAMP) and

the D2 isoform of vacuolar (H+) ATPase (v-ATPase) V_o domain (Atp6v0d2).[28] Furthermore, osteoclasts recognize and physically attach to bone via αv- and β3-integrin.[29] After attaching to the bone, osteoclasts dissolve the bone matrix by acidification, followed by the secretion of proteolytic enzymes such as cathepsin K.[30] On the other hand, calcitonin receptor (CTR) on osteoclasts regulates calcium homeostasis and conserves bone mass.[31] To confirm the inhibitory effect of **K7**, we investigated the expression of marker genes required for osteoclast differentiation and bone resorption by RT-PCR. As shown in Figure 3, **K7** significantly decreased the RANKL-induced expression of DC-STAMP, Atp6v0d2, αv- and β3-integrin, cathepsin K and CTR.

2.5. Downregulation of RANKL-induced NFATc1 expression via MAPK and NF-κB pathways

NFATc1 plays a pivotal role in RANKL-induced up-regulation of marker genes associated with osteoclast differentiation and activation.[6] Thus, we investigated the effect of **K7** on RANKL-induced expression of NFATc1. **K7** completely blocked the induction of NFATc1 by RANKL (Fig. 4A). To investigate whether down-regulation of NFATc1 protein levels is involved in the anti-osteoclastogenic effects of **K7**, we overexpressed a constitutively active form of NFATc1 in BMMs using a retroviral infection system. NFATc1-transduced BMMs were cultured with M-CSF and RANKL, in the absence or presence of **K7** for 4 days. As shown in Figure 4B, NFATc1 overexpression completely reversed the inhibition of osteoclast formation in the presence of **K7**. These data indicated that the inhibitory effect of **K7** on osteoclast differentiation was due mainly to reduction in NFATc1 expression.

It is well known that RANKL stimulates multiple intracellular signaling cascades including MAPK pathways (ERK, SAPK/JNK, and p38) and the NF-κB pathway.[32–35] These signaling cascades lead to the induction NFATc1 and subsequent osteoclast differentiation.[36] To define the molecular mechanism of the inhibitory effects of **K7** on osteoclastogenesis, we next examined the effects of **K7** on the early signaling pathways induced by RANKL in BMMs. As shown in Figure 4C and D, activation of ERK and p38 MAPK was observed after RANKL treatment, which was suppressed on pretreatment with **K7**. These results suggested the involvement of ERK and p38 MAP kinase pathways in the anti-osteoclastogenic effect of **K7**. We also examined its effect on the NF-κB signaling pathway. Upon RANKL stimulation, NF-κB is activated through IKK activation and the subsequent phosphorylation and degradation of IκB.[37] RANKL stimulation led to the degradation of IκB, and **K7** inhibited this process (Fig. 4E). Taken together, **K7**

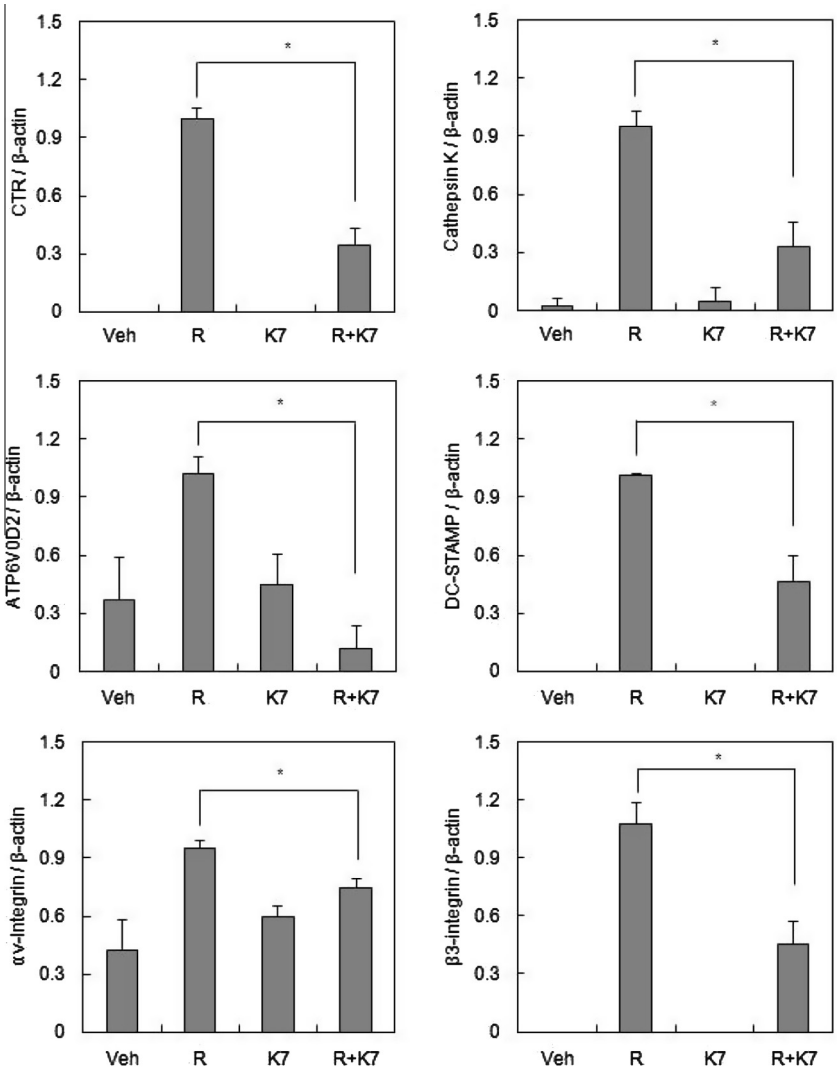

Figure 3. **K7** suppresses mRNA expression of osteoclastogenic genes induced by RANKL. BMMs were cultured for 4 days in the absence or presence of the 10 μM of **K7** with RANKL (100 ng/mL) and M-CSF (30 ng/mL). Total RNA was then isolated from the cells and cDNA templates were prepared. mRNA expression was determined by RT-PCR using specific primers designed for each gene. Veh, vehicle; R, RANKL ($^*p$ <0.05). Data are expressed as mean ± SD of three independent experiments.

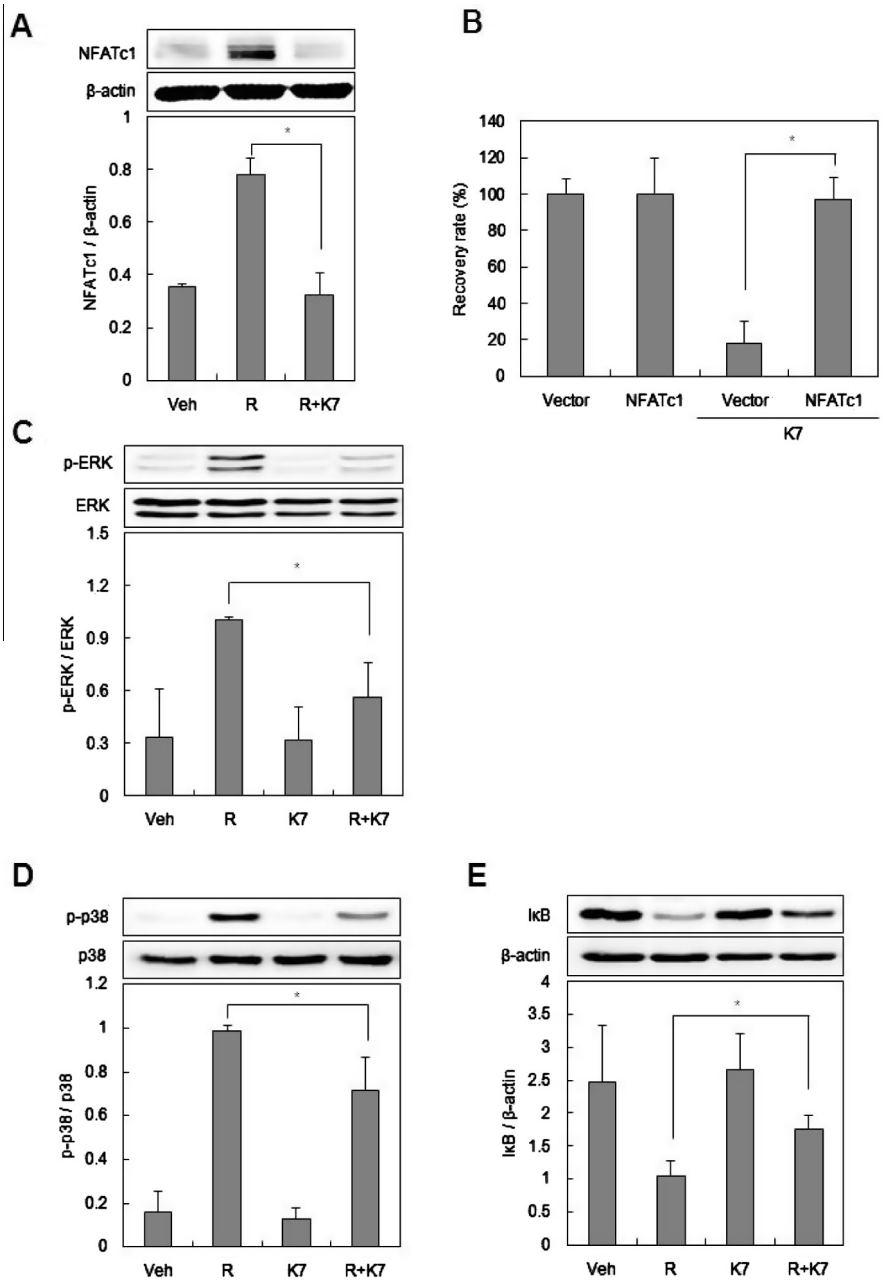

Figure 4. **K7** inhibits RANKL-induced NFATc1 expression and signaling pathways. (A) BMMs were pretreated with **K7** (10 μM) for 30 min, and then stimulated with 200 ng/mL RANKL for 24 h in the presence of M-CSF (30 ng/mL). Cell lysates were the subjected to Western blot analysis with NFATc1 antibody. (B) BMMs were infected through the retrovirus packaging system. After puromycin selection, cells were collected and cultured for 4 days with M-CSF (30 ng/mL) and RANKL (100 ng/mL) in the presence or absence of **K7** (10 μM). Cells were fixed and stained for TRAP. $TRAP^+$ MNCs were counted. (C–E) BMMs were preincubated in the absence or presence of 10 μM of **K7** for 30 min, and then treated with or without 200 ng/mL of RANKL for 15 min (for ERK, p38, and IκB). Cell lysates were then subjected to Western blot analysis with the indicated antibodies. Antibodies specific for ERK, p38, IκB or β-actin were used to normalize the cell extracts, respectively. Veh, vehicle; R, RANKL; N.S., not significant ($^*p$ <0.05). Data are expressed as mean ± SD of three independent experiments.

inhibited RANKL-induced expression of NFATc1, which is attributable to the modulation of ERK, p38 MAPK, and NF-κB signaling pathways.

2.6. Prevention of LPS-induced osteoclastogenesis in vivo

We evaluated the in vivo effect of **K7** on osteoclast formation using the lipopolysaccharide (LPS)-challenged mouse model. LPS stimulates bone loss by increasing the number of osteoclasts in vivo.[38] Firstly, we examined the effect of **K7** on LPS-induced osteoclast formation in a culture system. As shown in Figure 5A, **K7** suppressed LPS-induced osteoclast formation in vitro. Next, we injected LPS into the supra calvarial region of mice treated with or without **K7**. TRAP staining of whole calvariae showed that LPS markedly increased osteoclast numbers. In contrast, treatment with **K7** significantly decreased the number of osteoclasts in LPS-injected calvarial bone (Fig. 5B and C). Taken together, these data indicated that **K7** has an inhibitory effect on LPS-induced osteoclastogenesis in vivo.

3. Discussion

5-LO converts AA into LTA_4, which is used to synthesize LTB_4 and the cysteinyl leukotrienes.[39,40] These metabolites of 5-LO are lipid signaling molecules that affect many physiological processes,

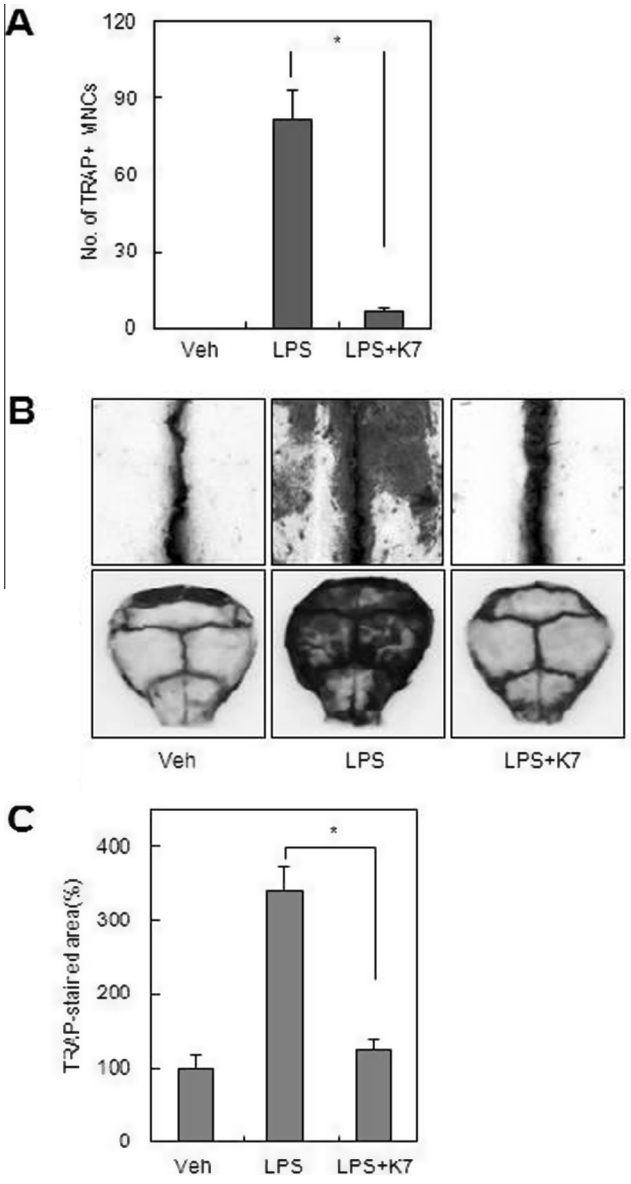

Figure 5. K7 inhibits LPS-induced osteoclast formation in vitro and in vivo. (A) BMMs were pre-incubated with M-CSF (30 ng/mL) and RANKL (100 ng/mL) for 36 h and then treated with M-CSF (30 ng/mL) and LPS (100 ng/mL) in the absence or presence of **K7** (10 μM) for 4 days. $TRAP^+$ cells that had more than 3 nuclei were counted. (B) Calvarias of mice that received vehicle, LPS or LPS plus **K7** (5 mg/kg) were subjected to TRAP staining. (C) $TRAP^+$ stained areas in calvarias were quantified by using the image J program. Results are representative of three independent sets of similar experiments. Veh, vehicle ($^*p$ <0.05).

including inflammation and allergy.[41,14] Recently 5-LO was suggested to be a direct regulator of bone metabolism. Furthermore, we have previously provided mechanistic insight by demonstrating that pharmacological blockade of 5-LO inhibits RANKL-induced osteoclastogenesis and bone loss.[42] Thus 5-LO inhibitors are considered as good therapeutic agents for bone-related diseases.

In this study, we showed that **K7**, a novel 5-LO inhibitor, prevented RANKL-induced osteoclastogenesis. It is well known that RANKL-induced activation of the NF-κB and MAPK pathways is required for osteoclastogenesis.[32–35] Further experiments suggested that the molecular mechanisms underlying the anti-osteoclastogenic effects of **K7** involved the ERK, p38 MAPK, and NF-κB signaling pathways. RANKL-induced expression of the transcription factor NFATc1, known to play a critical role in osteoclast development, was downregulated by **K7**. Because the exogenous expression of NFATc1 completely rescued the suppression of osteoclastogenesis by **K7**, we speculated that the inhibitory effect of **K7** on osteoclastogenesis attributes to the suppression of NFATc1 expression. During osteoclastogenesis, NFATc1 translocates from the cytoplasm to the nucleus to initiate transcription. In the nucleus, NFATc1 works together with other transcription factors, such as AP-1, PU.1, CREB, and microphthalmia-associated transcription factor (MITF). Accumulating evidence indicates that NFATc1 regulates the expression of osteoclast genes, including DC-STAMP, Atp6v0d2, αv- and β3-integrin, cathepsin K and CTR.[43–45] Consistent with this, **K7** also targets these molecules to regulate osteoclast differentiation.

LPS has been widely recognized as a key factor in the development of inflammatory bone loss.[37] Injection of LPS in mice evoked inflammatory bone loss by activation and differentiation of osteoclasts.[46,47] We verified that **K7** totally inhibited LPS-induced osteoclast formation in vivo in mouse calvaria, which was consistent with its in vitro effect. These data indicated that **K7** is a potential drug for osteoclast-mediated resorptive bone diseases.

The structure of **K7** is related to both the compounds DW 1350 and zileuton. DW 1350, *N*-hydroxy-4-{5-[4-(5-isopropyl-2-methyl-1,3-thiazol-4-yl)phenoxy]pentoxy}benzamidine, is a reported LTB_4 receptor antagonist for the prevention and treatment of osteoporosis.[48,49] DW 1350 showed inhibitory effects against osteoclast in terms of differentiation, formation, fusion and bone absorption. Zileuton, a 5-LO inhibitor, inhibits leukotrienes (LTB_4, LTC_4, LTD_4, and LTE_4) formation from AA (IC_{50} = 0.19 μM) (Fig. 6). However, zileuton did not have an inhibitory effect on osteoclasts (IC_{50} = >20 μM) in our experiment, even though the production of LTB_4 would be affected by this drug. Our compound **K7** successfully inhibited 5-LO (IC_{50} = l.72 μM) and suppressed RANKL-induced osteoclast formation (IC_{50} = 1.31 μM). The docking study of **K7** using the human X-ray crystal structure shown in Figure 1, showed similar pattern to the reported binding of zileuton. The 4-ethylaniline group nicely fitted into the bottom hole at the active site, and the amide NH was able to form hydrogen bonding with Ala672. In addition to zileuton similar parts, **K7** has *N*-hydroxy benzamidine moiety connected to pentoxy linker to amide NH. Therefore it is suggested that *N*-hydroxy benzamidine moiety connected to pentoxy or butoxy linker would be required for the inhibitory effect against osteoclast differentiation.

Depending on their actions at the ferric iron, which is at the center of the 5-LO active site, 5-LO inhibitors are conventionally classified into three categories: redox inhibitor, iron ligand inhibitor, and non-redox inhibitor.[50] During the process of enzyme activation, lipid peroxide converts inactive 5-LO with ferrous iron into active 5-LO with ferric iron. Redox inhibitors reduce ferric iron to the inactive ferrous iron. Iron ligand inhibitors have binding affinity to the ferric iron and block the binding ability of substrates without changing the iron state. Non-redox inhibitors compete with substrates for binding to 5-LO.[51] Given that redox and non-redox inhibitors may have qualitatively and quantitatively different effects on the products of 5-LO catalyzed reactions, we could not exclude the possibility that **K7** may act on 5-LO differently from zileuton. The mechanism by which **K7** inhibits 5-LO needs further investigation.

In conclusion, **K7** may be suitable for therapeutics in diseases characterized by excessive osteoclast-mediated bone resorption such as rheumatoid arthritis, osteoporosis or cancer-induced focal bone loss.

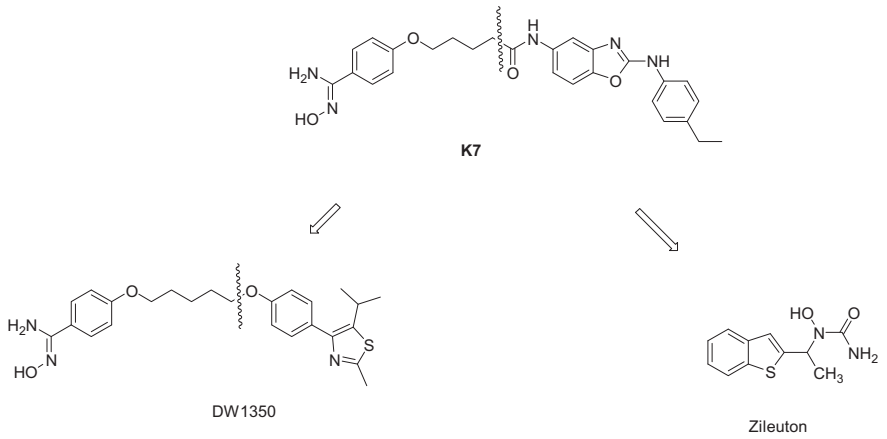

Figure 6. The structure of **DW 1350** and zileuton which are related to **K7**.

4. Experimental

4.1. Materials

Antibodies against ERK, phospho-ERK, IκB, β-actin, phospho-p38, p38, c-Fos and NFATc1 were purchased from Cell Signaling Technology (Beverly, MA, USA). All other reagents were from Sigma–Aldrich (St. Louis, MO, USA). ICR mice were obtained from Samtako Inc. (Seoul, Korea). Mice were maintained in the animal facility of the Sookmyung Women's University on a 12:12-h light–dark cycle, and were allowed food and water ad libitum. All experiments were performed in accordance with institutional guidelines approved by the Sookmyung Women's University Animal Care and Use Committee.

4.2. Synthesis of 5-(4-(*N*′-hydroxycarbamidoyl)-phenoxy)-*N*-(2-(4-substituted-phenylamino)benzo[*d*]oxazol-5-yl)pentanamide (2a–c)

The starting compounds **1a**–**c** were prepared as reported.[24] The compound **1a**–**c** (0.35 mmol) in 10 mL methanol was added 5% Pd/C and hydrogen, and stirred for 24 h at room temperature. The reaction mixture was filtered in celite, and the solvent was removed in vacuo to give **2a**–**c**.

4.2.1. 5-(4-(*N*′-Hydroxycarbamidoyl)-phenoxy)-*N*-(2-(4-ethyl-phenylamino)benzo[*d*]oxazol-5-yl)pentanamide (2a)

(0.079 g, 88%): Grey solid, mp 143–145 °C; ^{1}H NMR (400 MHz, Acetone-d_6) δ 9.170 (s, 1H), 7.737 (d, J = 8.4, 2H), 7.205 (d, J = 8.4, 2H), 7.036 (d, J = 8.8, 2H), 6.752 (s, 1H), 6.439 (d, J = 8.4, 1H), 4.443 (d, J = 10.4, 1H), 2.615 (q, J = 7.6, 2H), 1.210 (t, J = 7.6, 3H); HR-FABMS Calcd for $C_{15}H_{16}N_3O$ (M^++H): 254.1293, Found: 254.1292.

4.2.2. 5-(4-(*N*′-Hydroxycarbamidoyl)-phenoxy)-*N*-(2-(phenylamino)benzo[*d*]oxazol-5-yl)pentanamide (2b)

(0.361 g, 91%): Brown powder, mp 161–163 °C; ^{1}H NMR (400 MHz, Acetone-d_6) δ 9.271 (br s, 1H), 7.841 (d, J = 7.6 Hz, 2H), 7.357 (t, J = 7.6 Hz, 2H), 7.064–7.006 (m, 2H), 7.770 (d, J = 0.8 Hz, 1H), 6.456 (dd, J = 8.6, 2.2 Hz, 1H); HR-FABMS Calcd for $C_{13}H_{12}N_3O$ (M^++H): 226.0975, Found: 226.0978.

4.2.3. 5-(4-(*N*′-Hydroxycarbamidoyl)-phenoxy)-*N*-(2-(4-methoxy-phenylamino)benzo[*d*]oxazol-5-yl)pentanamide (2c)

(0.067 g, 14%): Brown powder, mp 156–158 °C; ^{1}H NMR (400 MHz, Acetone-d_6) δ 9.060 (br s, 1H), 7.737 (d, J = 9.2 Hz, 2H), 7.021 (d, J = 8.4 Hz, 1H), 6.942 (d, J = 9.2 Hz, 2H), 6.732 (d, J = 2 Hz, 1H), 6.418 (dd, J = 8.4, 2.4 Hz, 1H), 3.789 (s, 3H); HR-FABMS Calcd for C14H14N3O2 (M^++H): 256.1081, Found: 256.1084.

4.3. Synthesis of *N*-(2-(4-substituted phenylamino)benzo[*d*]oxazol-5-yl)-5-bromo-pentanamide (3a–c)

Compound **2a**–**c** (0.31 mmol), 5-bromovaleric acid (0.051 g, 0.28 mmol), and PyBOP (0.163 g, 0.31 mmol) in DMF(8 mL) were added to diisopropyl ethylamine (0.073 g, 0.57 mmol) in ice bath and the mixture was stirred for 16 h at room temperature. Ethyl acetate 8 mL was added and the mixture was washed with 10% HCl, saturated $NaHCO_3$ and NaCl solution. The organic layer was dried over $MgSO_4$ and the solvent was removed in vacuo. Column chromatography (EtOAc/hexane = 2:1) gave compound **3a**–**c**.

4.3.1. *N*-(2-(4-Ethylphenylamino)benzo[*d*]oxazol-5-yl)-5-bromo-pentanamide (3a)

(0.054 g, 46%): Pale brown powder, mp 196–198 °C; ^{1}H NMR (400 MHz, Acetone-d_6) δ 9.360 (s, 1H), 9.152 (s, 1H), 7.871 (s, 1H), 7.755 (d, J = 8.4, 2H), 7.343 (d, J = 8.8, 1H), 7.266 (d, J = 8.4, 1H), 7.230 (d, J = 8.8, 2H), 3.546 (t, J = 6.6, 2H), 2.628 (q, J = 7.6, 2H), 2.428 (t, J = 7.2, 2H), 1.989–1.919 (m, 2H), 1.899–1.803 (m, 2H), 1.218 (t, J = 7.6, 3H); HR-FABMS Calcd for $C_{20}H_{23}BrN_3O_2$ (M^++H): 416.0974, Found: 416.0969.

4.3.2. *N*-(2-(Phenylamino)benzo[*d*]oxazol-5-yl)-5-bromo-pentanamide (3b)

(0.385 g, 62%): White powder, mp 166–168 °C; ^{1}H NMR (400 MHz, Acetone-d_6) δ 9.464 (br s, 1H), 9.165 (br s, 1H), 7.891–7.846 (m, 3H), 7.405–7.346 (m, 3H), 7.282 (d, J = 8.8 Hz, 1H), 7.061 (t, J = 7.4 Hz, 1H), 3.547 (t, J = 6.6, 2H), 2.430 (t, J = 7.4, 2H), 1.974–1.920 (m, 2H), 1.879–1.822 (m, 2H); HR-FABMS Calcd for $C_{18}H_{19}BrN_3O_2$ (M^++H): 388.0655, Found: 388.0648.

4.3.3. *N*-(2-(4-Methoxyphenylamino)benzo[*d*]oxazol-5-yl)-5-bromo-pentanamide (3c)

(0.055 g, 55%): White powder, mp 179–180 °C; ^{1}H NMR (400 MHz, Acetone-d_6) δ 9.266 (br s, 1H), 9.145 (br s, 1H), 7.844 (d, J = 1.6 Hz, 1H), 7.755 (d, J = 9.2 Hz, 2H), 7.330 (dd, J = 8.4, 2.5 Hz, 1H), 7.250 (d, J = 8.4 Hz, 1H), 6.965 (d, J = 9.2 Hz, 2H), 3.800 (s, 3H), 3.545 (t, J = 6.4 Hz, 2H), 2.425 (t, J = 7.2 Hz, 2H), 1.972–1.918 (m, 2H), 1.875–1.819 (m, 2H); HR-FABMS Calcd for $C_{19}H_{21}BrN_3O_3$ (M^++H): 418.0761, Found: 418.0756.

4.4. Synthesis of 5-(4-cyanophenoxy)-*N*-(2-(4-substituted phenylamino)benzo[*d*]-oxazol-5-yl)pentanamide (4a–c)

4-Cyanophenol (0.024 g, 0.20 mmol) in DMF 3 mL and K_2CO_3 (0.032 g, 0.23 mmol were stirred at 50–55 °C for 30 min. Then compound **3a–c** (0.15 mmol) in DMF 4 mL was added and stirred at 60 °C for 5 h. After the reaction mixture was cooled to rt, Ethyl acetate 7 mL was added and washed with water, and saturated NaCl solution. The organic layer was dried over $MgSO_4$ and the solvent was removed in vacuo. Washing with ether gave **4a–c**.

4.4.1. 5-(4-Cyanophenoxy)-*N*-(2-(4-ethyl phenylamino)benzo[*d*]-oxazol-5-yl)pentanamide (4a)

(0.036 g, 52%): Pale yellow powder, mp 200–203 °C; ^{1}H NMR (400 MHz, Acetone-d_6) δ 9.358 (s, 1H), 9.151 (s, 1H), 7.874 (s, 1H), 7.755 (d, J = 8.4, 2H), 7.691 (d, J = 8.8, 2H), 7.339 (d, J = 8.6, 1H), 7.264 (d, J = 8.4, 1H), 7.231 (d, J = 8.4, 2H), 7.122 (d, J = 9.2, 2H), 4.167 (t, J = 6.0, 2H), 2.627 (q, J = 7.6, 2H), 2.473 (t, J = 7.0, 2H), 1.907–1.876 (m, 4H), 1.218 (t, J = 7.6, 3H); HR-FABMS Calcd for $C_{27}H_{27}N_4O_3$ (M^++H): 455.2083, Found: 455.2080.

4.4.2. 5-(4-Cyanophenoxy)-*N*-(2-(phenylamino)benzo[*d*]-oxazol-5-yl)pentanamide (4b)

(0.259 g, 63%): white powder, mp 181–182 °C; ^{1}H NMR (400 MHz, Acetone-d_6) δ 9.464 (br s, 1H), 9.167 (br s, 1H), 7.893 (d, J = 2 Hz, 1H) 7.872–7.847 (m, 2H), 7.692 (d, J = 8.8 Hz, 2H), 7.405–7.343 (m, 3H), 7.281 (d, J = 8.8, 1H), 7.122 (d, J = 8.8, 2H), 7.061 (t, J = 7.4 Hz, 1H), 4.168 (t, J = 6 Hz, 2H), 2.476 (t, J = 6.8 Hz, 2H), 1.909–1.892 (m, 4H); HR-FABMS Calcd for $C_{25}H_{23}N_4O_3$ (M^++H): 427.1765, Found: 427.1761.

4.4.3. 5-(4-Cyanophenoxy)-*N*-(2-(4-methoxyphenylamino) benzo[*d*]-oxazol-5-yl)pentanamide (4c)

(0.029 g, 48%): white powder, mp 213–215 °C; ^{1}H NMR (400 MHz, Acetone-d_6) δ 9.263 (br s, 1H), 9.146 (br s, 1H), 7.849 (s, 1H), 7.755 (d, J = 9.2 Hz, 2H), 7.691 (d, J = 8.8 Hz, 2H), 7.329 (d, J = 8.4 Hz, 1H), 7.248 (d, J = 8.4 Hz, 1H), 7.122 (d, J = 9.2 Hz, 2H), 6.965 (d, J = 8.8 Hz, 2H), 4.167 (t, J = 6.2 Hz, 2H), 3.800 (s, 3H), 2.470 (t, J = 7 Hz, 2H), 1.905–1.874 (m, 4H); HR-FABMS Calcd for $C_{26}H_{25}N_4O_4$ (M^++H): 457.1870, Found: 457.1871.

4.5. Synthesis of 5-(4-*N*′-hydroxycarbamimidoyl)-phenoxy)-*N*-(2-(4-ethyl-phenylamino)benzo[*d*]oxazol-5-yl)pentanamide (5a–c)

Compound **4a–c** (0.07 mmol) in 5 mL methanol was added to hydroxylamine 50% solution in water (0.54 mL, 0.35 mmol), and refluxed for 16 h. After the reaction mixture was cooled to 40 °C, water was added slowly to give the crystal. Washing with ether gave **5a–c**.

4.5.1. 5-(4-*N*′-Hydroxycarbamimidoyl)-phenoxy)-*N*-(2-(4-ethyl-phenylamino)benzo[*d*]oxazol-5-yl)pentanamide (5a) (K7)

(0.024 g, 69%): White powder, mp 191–196 °C; ^{1}H NMR (400 MHz, Acetone-d_6) δ 9.364 (s, 1H), 9.162 (s, 1H), 8.693 (s, 1H), 7.881 (s, 1H), 7.753 (d, J = 8.8, 2H), 7.643 (d, J = 9.2, 2H), 7.349 (d, J = 8.0, 1H), 7.263 (d, J = 8.4, 1H), 7.229 (d, J = 8.8, 2H), 6.929 (d, J = 9.2, 2H), 5.371 (s, 2H), 4.070 (t, J = 6.0, 2H), 2.627 (q, J = 7.6, 2H), 2.467 (t, J = 7.2, 2H), 1.893–1.872 (m, 4H), 1.218 (t, J = 7.6, 3H); HR-FABMS Calcd for $C_{27}H_{30}N_5O_4$ (M^++H): 488.2298, Found: 488.2299.

4.5.2. 5-(4-*N*′-Hydroxycarbamimidoyl)-phenoxy)-*N*-(2-(phenylamino)benzo[*d*]oxazol-5-yl)pentanamide (5b)

(0.50 g, 18%): White powder, mp 202–203 °C; ^{1}H NMR (400 MHz, Acetone-d_6) δ 9.467 (br s, 1H), 9.178 (br s, 1H), 8.695 (br s, 1H), 7.901 (d, J = 2 Hz, 1H), 7.859 (d, J = 7.6, 2H), 7.643 (d, J = 8.8 Hz, 2H), 7.404–7.353 (m, 3H), 7.280 (d, J = 8.8, 1H), 7.061 (tt, J = 7.4, 0.8 Hz, 1H), 6.930 (d, J = 9.2 Hz, 2H), 5.373 (br s, 1H), 4.070 (t, J = 5.6 Hz, 2H), 2.470 (t, J = 7 Hz, 2H), 1.894–1.872 (m, 4H); HR-FABMS Calcd for $C_{25}H_{25}N_5O_4$ (M^++H): 460.1985, Found: 460.1988.

4.5.3. 5-(4-*N*′-Hydroxycarbamimidoyl)-phenoxy)-*N*-(2-(4-methoxy-phenylamino)benzo[*d*]oxazol-5-yl)pentanamide (5c)

(0.008 g, 30%) white powder, mp 200–202 °C; ^{1}H NMR (400 MHz, Acetone-d_6) δ 9.259 (s, 1H), 9.148 (s, 1H), 8.686 (s, 1H), 7.856 (s, 1H), 7.754 (d, J = 8.8 Hz, 2H), 7.642 (d, J = 8.8 Hz, 2H), 7.337 (d, J = 8.4 Hz, 1H), 7.247 (d, J = 8.8 Hz, 1H), 6.965 (d, J = 9.2 Hz, 2H), 6.929 (d, J = 9.2 Hz, 2H), 5.362 (br s, 2H), 4.070 (t, J = 6.2 Hz, 2H), 3.800 (s, 3H), 2.463 (t, J = 7.2 Hz, 2H), 1.905–1.870 (m, 4H); HR-FABMS Calcd for $C_{26}H_{27}N_5O_5$ (M^++H): 490.2090, Found: 490.2095.

4.6. Determination of 5-LO product LTC_4 formation

Mouse bone marrow-derived mast cells (BMMC) were obtained from male mice and cultured for up to 4 weeks in 50% enriched medium (RPMI containing 2 mM L-glutamine, 25 mM HEPES buffer, 2 mg/mL sodium bicarbonate, 100 units/mL penicillin G, 100 μg/mL streptomycin sulfate, and 0.25 μg/mL amphotericin B) supplemented with 10% fetal bovine serum (FBS) with IL-3 (Sigma I4144, 2 ng/mL). Three weeks after the culture, more than 98% of BMMC was found in the cells as assessed by staining method with toluidine blue.

4.6.1. Determination of LTC_4

BMMC were suspended in the enriched medium at a cell density of 1×10^6 cells/mL, and were then incubated in a humidified 5% CO_2 incubator with or without sample in DMSO (final DMSO concentration was <0.5%) for 30 min at 37 °C. After the stimulation with stem cell factor (SCF, Sigma S9915, 100 ng/mL) for 20 min, the LTC_4 release in supernatants was measured by an enzyme immunoassay kit (Cayman Chemical, Ann Arbor, MI, USA) according to the manufacturer's instructions. All the experiments were carried out in triplicate and the inhibition of LTC_4 release was determined by calculating % reduction of LTC_4 release.

4.7. Molecular modeling

The 3-dimensional structure of the **K7** was generated using Concord and energy minimized with MMFF94s force field and MMFF94 charge until the rms of Powell gradient was 0.05 kcal mol^{-1} A^{-1} in SYBYL-X 2.0 (Tripos Int., St. Louis, MO, USA). Flexible docking study on the human 5-LO crystal structure (PDB ID: 3V99) was carried out using GOLD v.5.2 (Cambridge Crystallographic Data Centre, Cambridge, UK), which uses a genetic algorithm (GA) and allows for full ligand flexibility.[25] The binding site was specified as 10 Å around the arachidonic acid complexed in PDB 3V99. The coordination geometry of metal ion Fe^{2+} was set to be octahedral in GOLD.[52] **K7** was docked with the GoldScore scoring function, and the other parameters remained as default. All the computation calculations were undertaken on an Intel® Xeon™ Quad-core 2.5 GHz workstation with Linux Cent OS release 5.5.

4.8. Cells and culture system

Bone marrow cells were obtained from the long bones of 4- to 6-week-old male mice. Bone marrow cells were cultured in alpha-minimal essential medium (MEM) containing 10% FBS with the presence of M-CSF (10 ng/mL, R&D systems, Inc., Minneapolis, MN, USA) overnight. Non-adherent cells were harvested and cultured with M-CSF (30 ng/mL) for 3 days to generate the bone marrow-derived macrophages (BMMs). After 3 days, adherent cells

were used as osteoclast precursors. All cells were cultured in alpha-MEM with 10% FBS at 37 °C in 5% CO_2 incubator. To examine osteoclast formation, BMMs were treated with reagents in the presence of M-CSF (30 ng/mL) and RANKL (100 ng/mL, PeproTech, Rocky Hill, NJ, USA). Cells were fixed and stained for TRAP, a marker enzyme of osteoclasts. The number of $TRAP^+$ cells with more than 3 or 5 nuclei was counted under a light microscope.

4.8.1. MTT assay

BMMs were cultured with M-CSF (30 ng/mL, R&D) and the reagents in alpha-MEM medium for 4 days, MTT solution was then added and incubated in the dark. After 5 h solubilization buffer (10% SDS in 0.01 M HCl) was added and cultured overnight. The proliferation was measured at an OD value of 570 nm.

4.8.2. RT-PCR analysis

Total RNA was extracted from BMMs by Easy-Blue (iNtRON Biotechnology, Inc.). cDNA was synthesized from total RNA by using RevertAid™ first strand cDNA synthesis Kit (Fermentas, EU) and amplified using PCR. Primers for osteoclastogenic genes used in this study are as follows: calcitonin receptor (CTR), 5′-tttcaagaaccttagctgccagag-3′ (forward), 5′-caaggcacggacaatgttgagaag-3′ (reverse); cathepsin K, 5′-cttccaatacgtgcagcaga-3′ (forward), 5′-acgcaccaatatcttgcacc-3′ (reverse); β-actin, 5′-tttgatgtcacgcacgatttcc-3′ (forward), 5′-tgtgatggtgggaatgggtcag-3′ (reverse); Atp6v0d2, 5′-tcagatctcttcaaggctgtgctg-3′ (forward), 5′-gtgccaaatgagttcagagtgatg-3′ (reverse); DC-STAMP, 5′-tggaagttcacttgaaactacgtg-3′ (forward), 5′-ctcggtttcccgtcagcctctctc-3′ (reverse); αv-Integrin, 5′-cctcagagagggagatgttcacac-3′ (forward), 5′-aactgccaagatgatcacccacac-3′ (reverse) β3-Integrin, 5′-gatgacatcgagcaggtgaaagag-3′ (forward), 5′-ccggtcatgaatggtgatgagtag-3′ (reverse). The PCR program was as follows: 32 (β3-Integrin), 30 (Atp6v0d2, DC-STAMP), 28 (CTR, αv-Integrin), 22 (Cathepsin k, β-actin) cycles, after an initial denaturation step at 94 °C for 3 min, then denaturation at 94 °C for 30 s, annealing at 60 (αv-Integrin), 59 (Atp6v0d2), 58 (CTR, Cathepsin k, β3-Integrin, β-actin and DC-STAMP)°C for 45 s, and extension at 72 °C for 60 s, with a final extension at 72 °C for 10 min.

4.8.3. Immunoblot analysis

Total cell lysates were isolated, separated by SDS–PAGE, and transferred onto Immobilon-P membranes (Millipore, Bedford, MA, USA). The membranes were blocked with 5% non-fat-milk in PBS-T (PBS 0.1% Tween 20), and then immunostained with specific antibodies and immuno-reactivity was detected with ECL solution (Amersham Biosciences, Buckinghamshire, UK) using an LAS3000 luminescent image analyzer (FUJIFILM Co., Tokyo, Japan).

4.8.4. Retroviral gene transduction

Plat-E retroviral packaging cells were seeded in a culture dish 1 day before transfection. Next day, PMX-puro GFP (GFP-vector) or PMSCV-GFP CA-NFATc1 (CA-NFATc1) was transfected into plat-E cells using Lipofectamine 2000 CD (Invitrogen by Life Technologies, Inc. Grand Island, NY, USA). After 2 days, culture supernatants of the retrovirus-producing cells were collected. BMMs were seeded with culture supernatants of PMX-puro GFP or PMSCV-FPNFATc1virus producing plat-E cells together with polybrene (10 μg/mL, Santa Cruz Biotechnology, Inc. Buffalo, CA, USA) and M-CSF (30 ng/mL) overnight. Infected cells were then selected with puromycin (2 mg/mL) for 2 days and then further cultured with or without **K7** (10 μM) in the presence of M-CSF (30 ng/mL) and RANKL (100 ng/mL) for 4 days.

4.8.5. Bone resorption assay

BMMs were differentiated on dentine slices with M-CSF (30 ng/mL) and RANKL (100 ng/mL) for 4 days, and then **K7** (10 μM) was treated for 2 days in the presence of M-CSF and RANKL. The cells were removed from the dentin slice by wiping the surface, then slices were stained with toluidine blue (1 μg/mL, J.T. Baker, UK). And the numbers of pit formed by bone resorption on the dentin slices were counted.

4.9. In vivo experiment

To study the effects of **K7** on LPS-induced osteoclast formation in vivo, 6-week-old male mice were divided into three groups. Mice were administered **K7** (5 mg/kg, intraperitoneally (ip)) or vehicle (corn oil/DMSO = 9:1) daily. After a day, mice were injected subcutaneously with LPS (5 mg/kg) or vehicle (PBS) over calvarial bone. The mice were sacrificed 6 days after LPS injection, and whole calvariae were fixed in 4% paraformaldehyde and stained for TRAP.

4.10. Statistical analysis

Data represent the means and the ±SD from three independent experiments. Statistical analysis was performed by one-way analysis of variance followed by the Student's *t*-test. *p*-Value <0.05 was considered statically significant.

Acknowledgments

This research was supported by Basic Science Research program through the National Research Foundation of Korea (NRF) – South Korea funded by the Ministry of Education (NRF-2013R1A1A2062631) (to M. Yim), and by Grant from National Leading Research Lab (NLRL) program (2011-0028885) funded by the Ministry of Science, ICT and Future Planning (MSIP) and the National Research Foundation of Korea (NRF) – South Korea (to S. Choi).

References and notes

1. Väänänen, H. K.; Zhao, H.; Mulari, M.; Halleen, J. M. *J. Cell Sci.* **2000**, *113*, 377.
2. Rodan, G. A.; Martin, T. J. *Science* **2000**, *289*, 1508.
3. Boyle, W. J.; Simonet, W. S.; Lacey, D. L. *Nature* **2003**, *423*, 337.
4. Akiyama, T.; Dass, C. R.; Choong, P. F. *Mol. Cancer Ther.* **2008**, *7*, 3461.
5. Kajiya, M.; Giro, G.; Taubman, M. A.; Han, X.; Mayer, M. P.; Kawai, T. *J. Oral Microbiol.* **2010**. http://dx.doi.org/10.3402/jom.v2i0.5532. Published Online: November 8.
6. Takayanagi, H.; Kim, S.; Koga, T.; Nishina, H.; Isshiki, M.; Yoshida, H.; Saiura, A.; Isobe, M.; Yokochi, T.; Inoue, J.; Wagner, E. F.; Mak, T. W.; Kodama, T.; Taniquchi, T. *Dev. Cell* **2002**, *3*, 889.
7. Grigoriadis, A. E.; Wang, Z. Q.; Cecchini, M. G.; Hofstetter, W.; Felix, R.; Fleisch, H. A.; Wagner, E. F. *Science* **1994**, *266*, 443.
8. Funk, C. D. *Science* **2001**, *294*, 1871.
9. Samuelsson, B.; Rouzer, C. A.; Matsumoto, T. *Adv. Prostaglandin Thromboxane Leukot. Res.* **1987**, *17A*, 1.
10. Haeggstrom, J. Z. *J. Biol. Chem.* **2004**, *279*, 50639.
11. Sjöström, M.; Jakobsson, P. J.; Heimburger, M.; Palmblad, J.; Haeggstöm, J. Z. *Eur. J. Biochem.* **2001**, *268*, 2578.
12. Montuschi, P. *Mini-Rev. Med. Chem.* **2008**, *8*, 647.
13. Gheorghe, K. R.; Korotkova, M.; Catrina, A. I.; Backman, L.; af Klint, E.; Claesson, H. E.; Rådmark, O.; Jakobsson, P. J. *Arthritis Res. Ther.* **2009**. http://dx.doi.org/10.1186/ar2717. Published online: June 4.
14. Manigrasso, M. B.; O'Connor, J. P. *Acta Orthop.* **2010**, *81*, 748.
15. Bonewald, L. F.; Flynn, M.; Qiao, M.; Dallas, M. R.; Mundy, G. R.; Boyce, B. F. *Adv. Exp. Med. Biol.* **1997**, *433*, 299.
16. Gallwitz, W. E.; Mundy, G. R.; Lee, C. H.; Qiao, M.; Roodman, G. D.; Raftery, M.; Gaskell, S. J.; Bonewald, L. F. *J. Biol. Chem.* **1993**, *268*, 10087.
17. Garcia, C.; Boyce, B. F.; Gilles, J.; Dallas, M.; Qiao, M.; Mundy, G. R.; Bonewald, L. F. *J. Bone Miner. Res.* **1996**, *11*, 1619.
18. Flynn, M. A.; Qiao, M.; Garcia, C.; Dallas, M.; Bonewald, L. F. *Calcif. Tissue Int.* **1999**, *64*, 154.
19. Gilbert, N. C.; Bartlett, S. G.; Waight, M. T.; Neau, D. B.; Boeglin, W. E.; Brash, A. R.; Newcomer, M. E. *Science* **2011**, *331*, 217.
20. Radmark, O. *J. Lipid Mediat. Cell Signal.* **1995**, *12*, 171.
21. Karelina, T. A.; Zhudenkov, K. V.; Demin, O. O.; Svetlichny, D. V.; Agoram, B.; Fairman, F.; Demin, O. V. *BMC Syst. Biol.* **2012**, *6*, 141.
22. Montuschi, P.; Peters-Golden, M. L. *Clin. Exp. Allergy* **2012**, *40*, 1732.

23. Lee, J. H.; Ahn, M. H.; Choi, E. H.; Park Choo, H. Y.; Lee, H. K.; Han, G. *Heterocycles* **2006**, *70*, 571.
24. Song, H.; Oh, S. R.; Lee, H. K.; Han, G.; Kim, J. H.; Chang, H. W.; Doh, K. E.; Rhee, H. K.; Park Choo, H. Y. *Bioorg. Med. Chem.* **2010**, *18*, 7580.
25. Singh, P.; Pooja *Bioorg. Med. Chem. Lett.* **2013**, *23*, 1433.
26. Shibakawa, A.; Yudoh, K.; Masuko-Hongo, K.; Kato, T.; Nishioka, K.; Nakamura, H. *Osteoarthr. Cartilage* **2006**, *13*, 679.
27. Asagiri, M.; Takayanagi, H. *Bone* **2007**, *40*, 251.
28. Kim, K.; Lee, S. H.; Kim, J. H.; Choi, Y.; Kim, N. *Mol. Endocrinol.* **2008**, *22*, 176.
29. Rodan, S. B.; Rodan, G. A. *J. Endocrinol.* **1997**, *154*, 47.
30. Wilson, S. R.; Peters, C.; Saftig, P.; Brömme, D.; Cathepsin, K. *J. Biol. Chem.* **2008**, *284*, 2584.
31. Lafont, A. G.; Wang, Y. F.; Chen, G. D.; Liao, B. K.; Tseng, Y. C.; Huang, C. J.; Hwang, P. P. *J. Bone Miner. Res.* **2011**, *26*, 1072.
32. Zheng, H.; Yu, X.; Collin-Osdoby, P.; Osdoby, P. *J. Biol. Chem.* **2006**, *281*, 15809.
33. Matsumoto, M.; Sudo, T.; Maruyama, M.; Osada, H.; Tsujimoto, M. *FEBS Lett.* **2000**, *486*, 23.
34. Ikeda, F.; Nishimura, R.; Matsubara, T.; Tanaka, S.; Inoue, J.; Reddy, S. V.; Hata, K.; Yamashita, K.; Hiraga, T.; Watanabe, T. *J. Clin. Invest.* **2004**, *114*, 475.
35. Ishida, N.; Hayashi, K.; Hoshijima, M.; Ogawa, T.; Koga, S.; Miyatake, Y.; Kumegawa, M.; Kimura, T.; Takeya, T. *J. Biol. Chem.* **2002**, *277*, 41147.
36. Crottia, T. N.; Flannery, M.; Walsh, N. C.; Fleming, J. D.; Goldring, S. R.; McHugh, K. P. *PMC* **2006**, *372*, 92.
37. Oeckinghaus, A.; Ghosh, S. *Cold Spring Harb. Perspect. Biol.* **2009**, *1*, a000034.
38. Sakuma, Y.; Tanaka, K.; Suda, M.; Komatsu, Y.; Yasoda, A.; Miura, M.; Ozasa, Ami.; Narumiya, Shuh.; Sugimoto, Y.; Ichikawa, A.; Ushikubi, F.; Nakao, K. *Infect. Immun.* **2000**, *68*, 6819.
39. Gijón, M. A.; Zarini, S.; Murphy, R. C. *J. Lipid Res.* **2007**, *48*, 716.
40. Murphy, R. C.; Gijón, M. A. *Biochem. J.* **2007**, *405*, 379.
41. Krönke, G.; Katzenbeisser, J.; Uderhardt, S.; Zaiss, M. M.; Scholtysek, C.; Schabbauer, G.; Zarbock, A.; Koenders, M. I.; Axmann, R.; Zwerina, J.; Baenckler, H. W.; van den Berg, W.; Voll, R. E.; Kühn, H.; Joosten, L. A.; Schett, G. *J. Immunol.* **2009**, *183*, 3383.
42. Lee, J. M.; Park, H.; Noh, A. L.; Kang, J. H.; Chen, L.; Zheng, T.; Lee, J.; Ji, S. Y.; Jang, C. Y.; Shin, C. S.; Ha, H.; Lee, Z. H.; Park, H. Y.; Lee, D. S.; Yim, M. *J. Immunol.* **2012**, *189*, 5284.
43. Kim, K.; Kim, J. H.; Lee, J.; Jin, H. M.; Lee, S. H.; Fisher, D. E.; Kook, H.; Kim, K. K.; Choi, Y.; Kim, N. *J. Biol. Chem.* **2005**, *280*, 35209.
44. Matsumoto, M.; Kogawa, M.; Wada, S.; Takayanagi, H.; Tsujimoto, M.; Katayama, S.; Hisatake, K.; Nogi, Y. *J. Biol. Chem.* **2004**, *279*, 45969.
45. Yagi, M.; Ninomiya, K.; Fujita, N.; Suzuki, T.; Iwasaki, R.; Morita, K.; Hosogane, N.; Matsuo, K.; Toyama, Y.; Suda, T.; Miyamoto, T. *J. Bone Miner. Res.* **2007**, *22*, 992.
46. Zou, W.; Bar-Shavit, Z. *J. Bone Miner. Res.* **2002**, *17*, 1211.
47. Hou, G. Q.; Guo, C.; Song, G. H.; Fang, N.; Fna, W. J.; Chen, X. D.; Yuan, L.; Wang, Z. Q. *Int. J. Mol. Med.* **2013**, *32*, 503.
48. Suh, H.; Lee, J.; Kim, P.; Hwang, Y.; Ryu, J.; Chung, Y.; Kim, E.; Kim, D.; Park, Y. WO 2,003,007,947.
49. Lee, J.; Ahn, S.; Jin, Y.; Park, J.; Shin, D.; Cho, E.; Chanf, H.; Jung, Y. WO 2,006,004,368.
50. Werz, O.; Steinhilber, D. *Pharmacol. Ther.* **2006**, *112*, 701.
51. Pergola, C.; Werz, O. *Expert Opin. Ther. Pat.* **2010**, *20*, 355.
52. Rådmark, O.; Werz, O.; Steinhilber, D.; Samuelsson, B. *Trends Biochem. Sci.* **2007**, *32*, 332.